Solution of Reactive Compressible Flows Using an Adaptive Wavelet Method

By

Z. J. Zikoski, S. Paolucci, and J. M. Powers

Aerospace and Mechanical Engineering
University of Notre Dame, Indiana 46556

Acknowledgement: This work is supported by NASA #NNX07AD10A.

61st Annual Meeting of the APS Division of Fluid Dynamics
San Antonio, Texas, November 23-25, 2008

Project Description

- An adaptive method is applied to problems in hypersonic propulsion.
- Compressible reactive Navier-Stokes model includes detailed chemical kinetics, multi-species transport, momentum and energy diffusion.
- These problems are typically multidimensional and contain a wide range of spatial and temporal scales.
- Our adaptive wavelet method allows this range of scales to be resolved while greatly reducing the required computer time and automatically produces verified solutions.

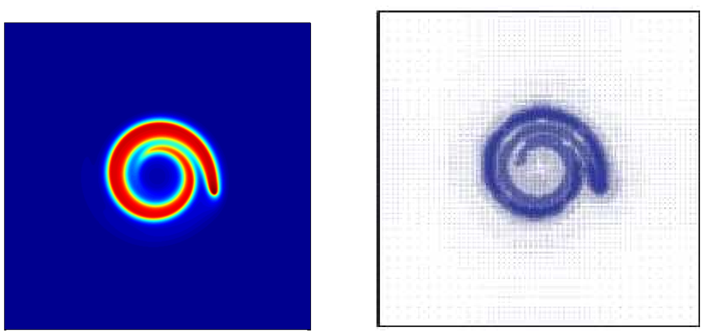

Figure: Flameball-vortex interaction–computed temperature field and adaptive grid.

Adaptive Wavelet Method

- The sparse wavelet transform (SWR) provides a multiscale representation of the solution:

$$u^J(\mathbf{x}) \;=\; \sum_{\mathbf{k}} u_{J_0,\mathbf{k}} \Phi_{j_0,\mathbf{k}}(\mathbf{x}) + \sum_{j=j_0}^{J-1} \sum_{\{\boldsymbol{\lambda}\,:\,|d_{j,\boldsymbol{\lambda}}|\geq\varepsilon\}} d_{j,\boldsymbol{\lambda}} \Psi_{j,\boldsymbol{\lambda}}(\mathbf{x}). \quad (1)$$

- Since each basis function in (1) is related to a single dyadic grid point, the SWR is used to define a sparse grid of irregular points.
- Finite differences are used for derivative approximations.
- Solution is advanced in time using an explicit ODE solver with error control.

Compressible Reactive Flow

- n-dimensional code is implemented.
- Model includes detailed chemical kinetics, multi-component and thermal diffusion.
- Includes state-dependent specific heats and transport properties.
- CHEMKIN and TRANLIB libraries used for evaluation of transport properties, thermodynamics, and chemical source terms.

1-D Viscous Detonation

Initial conditions:

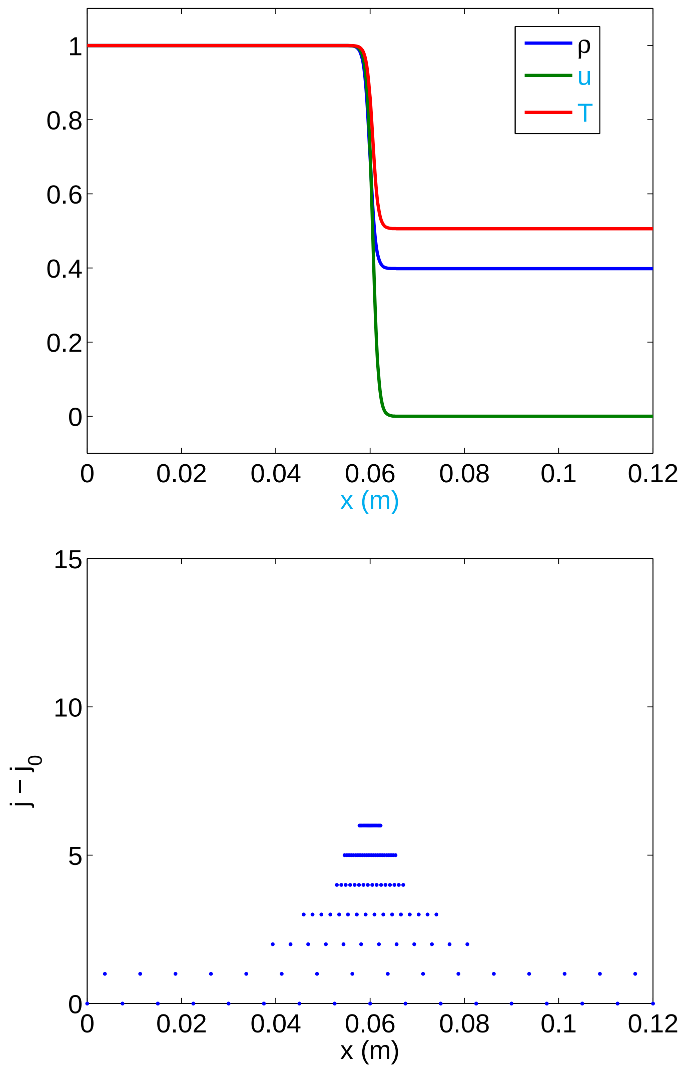

$2H_2 : 1O_2 : 7Ar$ mixture

9 species, 37 reactions

State 1: $0\ m \leq x < 0.06\ m$

$\rho_1 = 0.18075\ kg\ m^{-3}$

$P_1 = 35594\ Pa$

$u_1 = 487.34\ m\ s^{-1}$

State 2: $0.06\ m \leq x \leq 0.12\ m$

$\rho_2 = 0.072\ kg\ m^{-3}$

$P_2 = 7173\ Pa$

$u_2 = 0\ m\ s^{-1}$

Wavelet parameters:

$\epsilon = 1 \times 10^{-4}$

$p = 6, \quad n = 4$

$j_0 = 4, \quad J - j_0 = 15$

1-D Viscous Detonation (cont.)

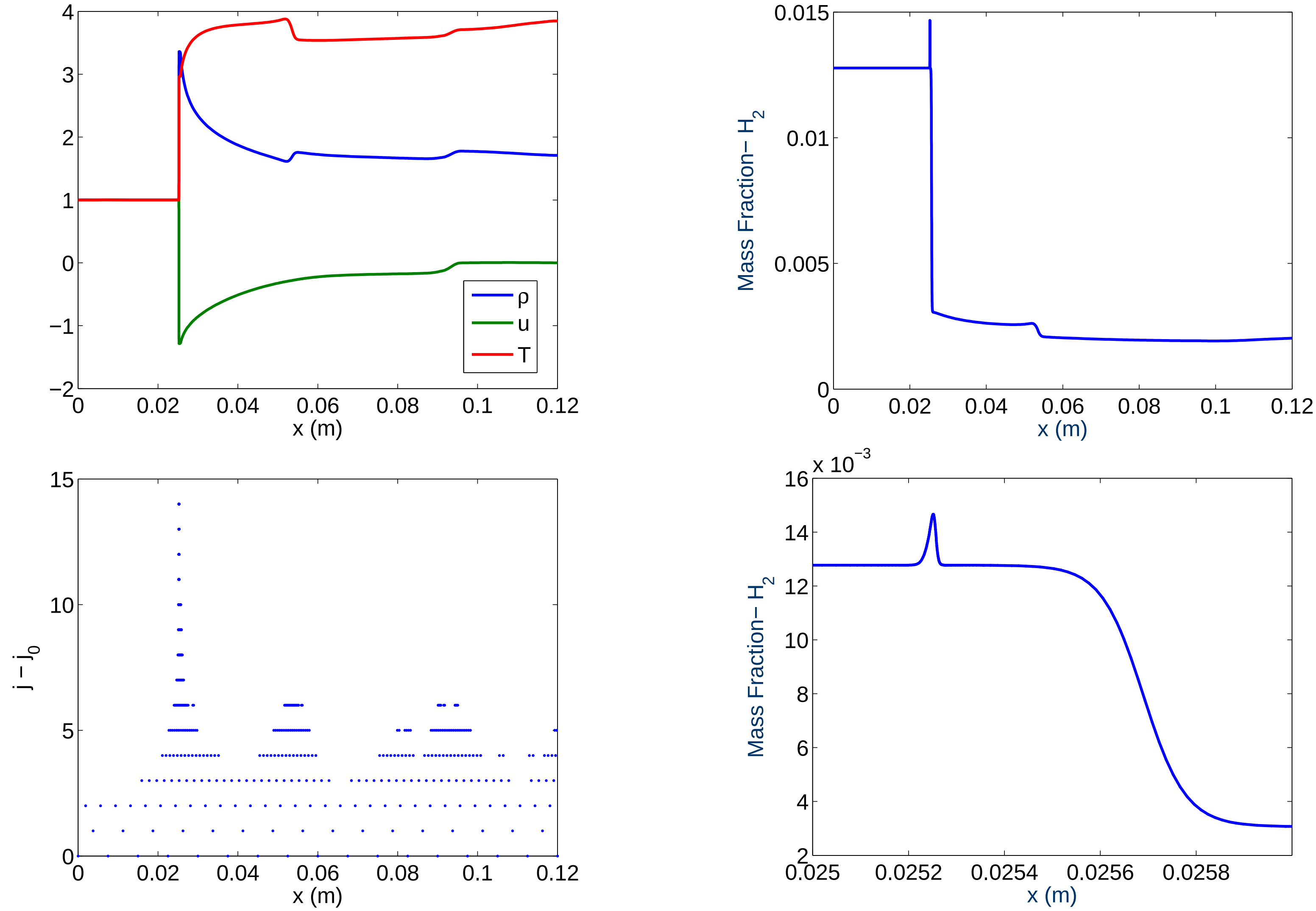

Demonstration of a Verified Solution: Taylor/Sedov Blast Wave

$78N_2 : 21O_2 : 1Ar$ (air) mixture
3 species, inert

$\rho(\mathbf{x}, 0) = 3 \times 10^{-5}\ gm\ cm^{-3}$
$\mathbf{u}(\mathbf{x}, 0) = 0\ cm\ s^{-1}$
$P_0 = 1 \times 10^4\ dyne\ cm^{-2}$
$P_{max}/P_0 = 50$
$P(\mathbf{x}, 0) = P_0 + P_{max} \exp(-500\|\mathbf{x}/L\|^2)$
$L = 100\ \mu m$

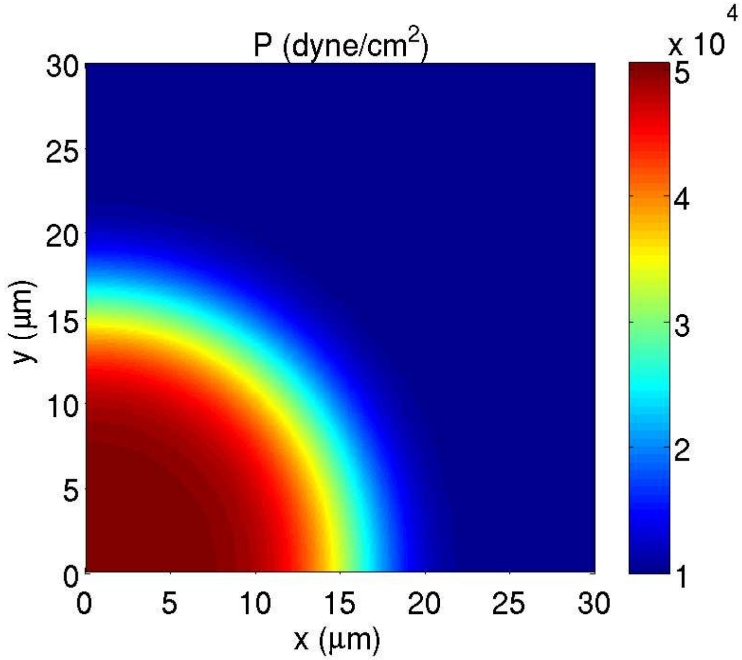

Wavelet parameters:

$\epsilon = 1 \times 10^{-3}$
$p = 6, \quad n = 4$
$j_0 = 3, \quad J - j_0 = 9$ (1-d), 6 (2-,3-d)

Demonstration of a Verified Solution: Taylor/Sedov Blast Wave (cont.)

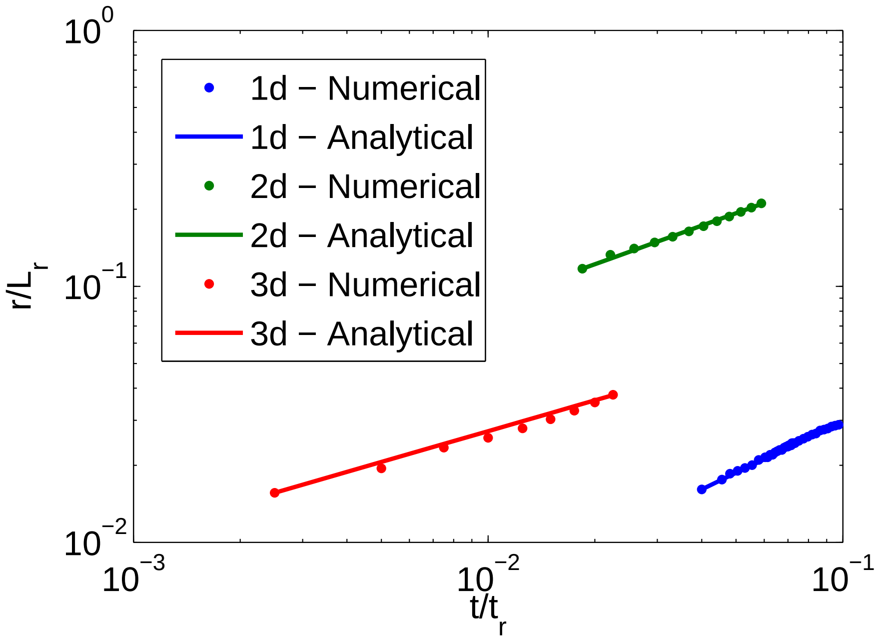

$$r(t) = \left(\frac{E}{\rho_0}\right)^a t^{2a}$$

$$a = (2+d)^{-1}$$

d	a-Analytical	a-Numerical
1	0.6667	0.6645
2	0.5000	0.4842
3	0.4000	0.3979

2-D Flameball

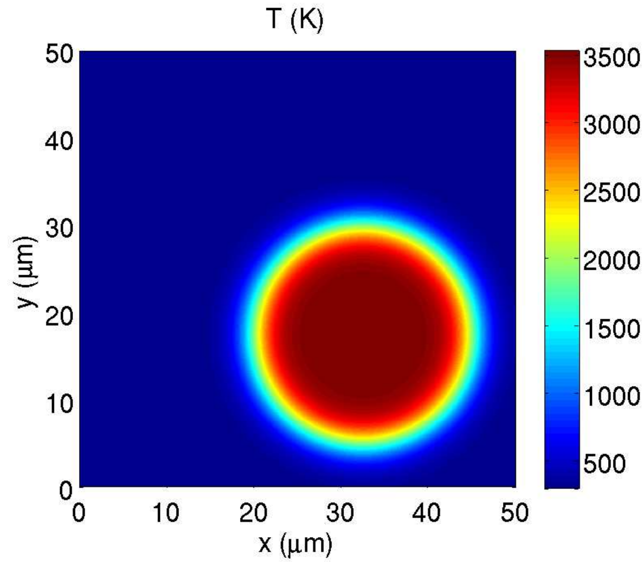

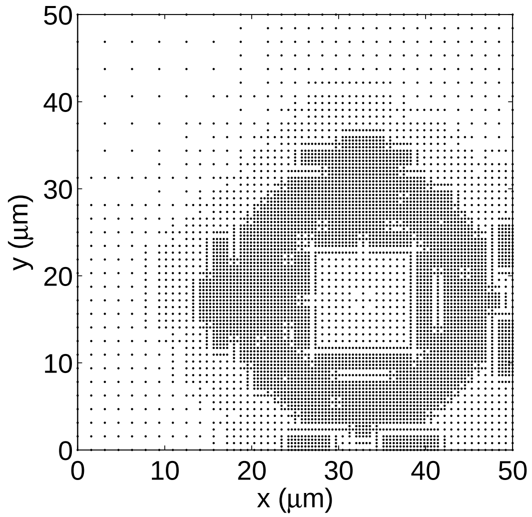

$2H_2 : 1O_2 : 7Ar$ mixture

9 species, 37 reactions

$\mathbf{x}_0 = (32.5\mu m,\ 17.5\mu m)$

$r = \|\mathbf{x} - \mathbf{x}_0\|_2$

$\mathbf{u} = 0\ cm\ s^{-1}$

State 1: $r > 12.5\ \mu m$

$\rho_1 = 1.265\ kg\ m^{-3}$

$T_1 = 300\ K$

State 2: $r \leq 12.5\ \mu m$

$\rho_2 = 1.265\ kg\ m^{-3}$

$T_2 = 3530\ K$

Wavelet parameters:

$\epsilon = 1 \times 10^{-3}$

$p = 6, \quad n = 4$

$j_0 = 3, \quad J - j_0 = 7$

2-D Flameball (cont.)

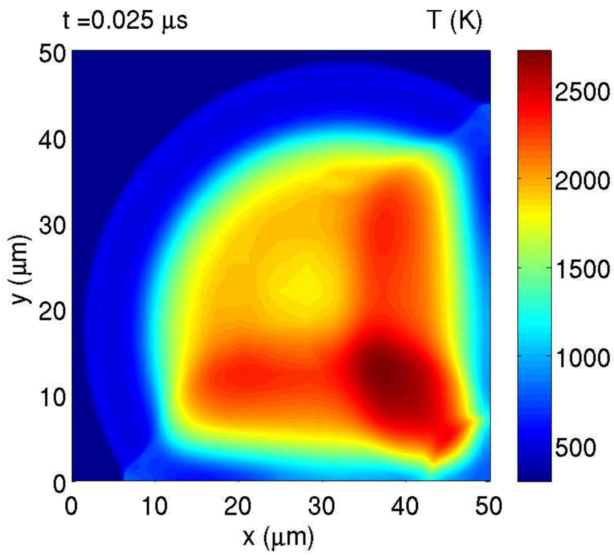

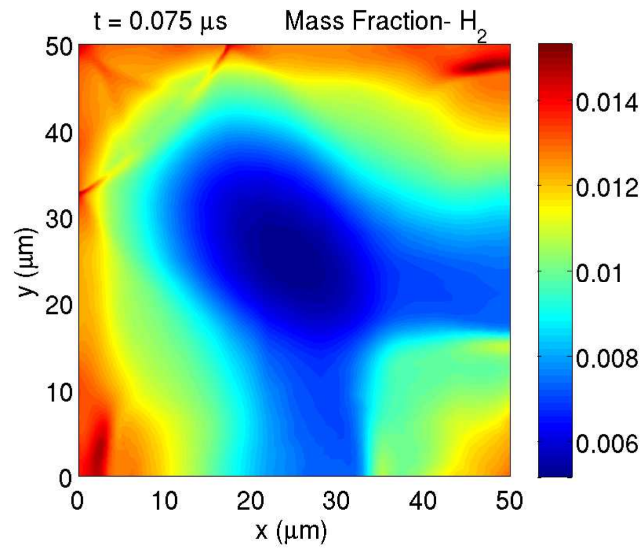

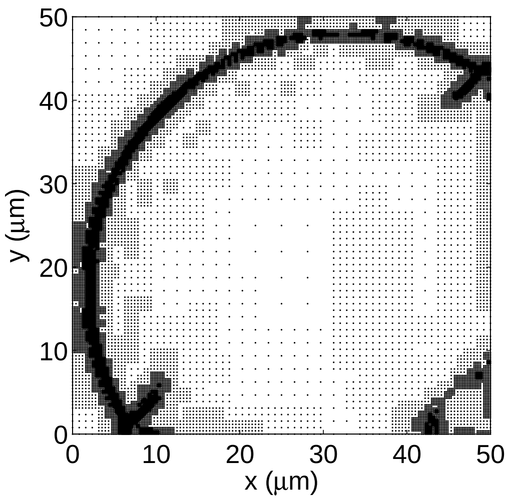

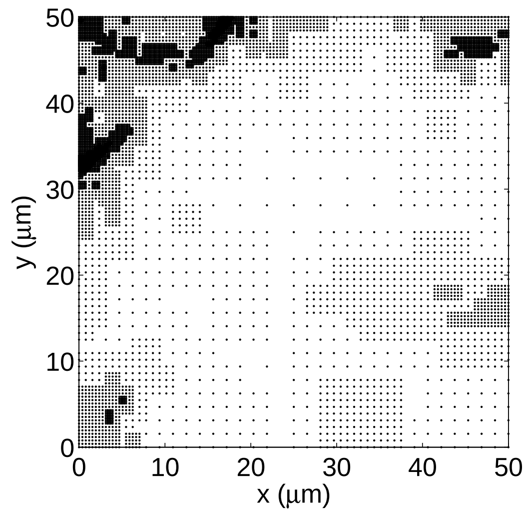

Runtime Comparisons

Case	N_a	N_f	t_{adap} (hr)	t_{full} (hr)	Speedup
1-D Detonation	275	2.6×10^5	343	3.3×10^5	950
1-D Blast Wave	305	4.1×10^3	0.06	0.8×10^0	13
2-D Blast Wave	2566	2.6×10^5	0.83	8.5×10^1	102
3-D Blast Wave	23084	1.3×10^8	29.5	1.7×10^5	5800
2-D Flameball	12784	1.0×10^6	29	2.4×10^3	82

N_a - average number of points in adaptive grid
N_f - total number of points in equivalent uniform grid
t_{adap} - runtime of adaptive routine $[CPU\ hr]$
t_{full} - est. runtime of routine with equivalent full grid $[CPU\ hr]$
Speedup - t_{full}/t_{adap}

Summary

- An adaptive wavelet method is successfully applied to compressible reacting flows in multiple dimensions.
- The method is shown to provide large speedup in problems in multiple dimensions or with a wide range of scales.
- Verified solutions with large geometries require large computational resources, even with an adaptive method.
  Powers and Paolucci *AIAA J* 2005; Powers *JPP* 2006

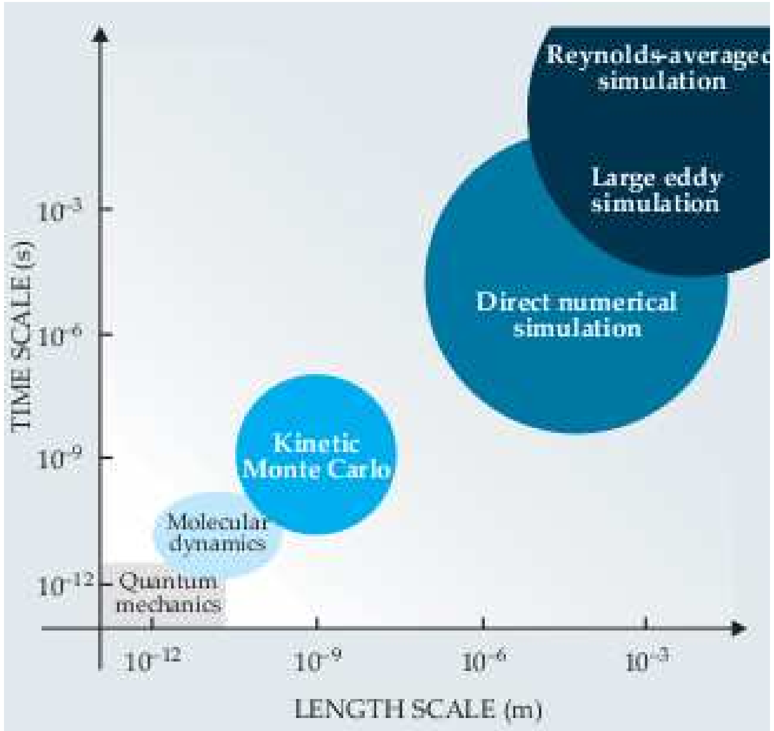

"Research needs for future internal combustion engines,"
Physics Today, Nov. 2008, pp 47-52.

Wavelet Approximation in Domain $[0,1]^d$

Approximation of $u(\mathbf{x})$ by the interpolating wavelet, a multiscale basis, on $\mathbf{x} \in [0,1]^d$ is given by

$$u(\mathbf{x}) \approx u^J(\mathbf{x}) = \sum_{\mathbf{k}} u_{j_0,\mathbf{k}} \Phi_{J_0,\mathbf{k}}(\mathbf{x}) + \sum_{j=J_0}^{J-1} \sum_{\lambda} d_{j,\lambda} \Psi_{j,\lambda}(\mathbf{x}),$$

where $\mathbf{x} \in \mathbb{R}^d$, $\lambda = (\mathbf{e}, \mathbf{k})$ and $\Psi_{j,\lambda}(\mathbf{x}) \equiv \Psi^{\mathbf{e}}_{j,\mathbf{k}}(\mathbf{x})$.

- Scaling function:

$$\Phi_{j,\mathbf{k}}(\mathbf{x}) = \prod_{i=1}^{d} \phi_{j,\mathbf{k}}(x_i),\ k_i \in \kappa_j^0$$

- Wavelet function:

$$\Psi^{\mathbf{e}}_{j,\mathbf{k}}(\mathbf{x}) = \prod_{i=1}^{d} \psi^{e_i}_{j,\mathbf{k}}(x_i),\ k_i \in \kappa_j^{e_i}$$

where $\mathbf{e} \in \{0,1\}^d \setminus \mathbf{0}$, $\psi^0_{j,k}(x) \equiv \phi_{j,k}(x)$ and $\psi^1_{j,k}(x) \equiv \psi_{j,k}(x)$, and $\kappa_j^0 = \{0, \cdots, 2^j\}$ and $\kappa_j^1 = \{0, \cdots, 2^j - 1\}$.

1-D Interpolating Scaling Function and Wavelet

Some properties of $\phi_{j,k}$ and $\psi_{j,k}$ of order p ($p \in \mathbb{N}$, even):

- $\phi_{j,k}$ is defined through $\phi(2^j x - k)$ where $\phi(x) = \int \varphi_p(y)\varphi_p(y-x)dy$, the auto-correlation of the Daubechies wavelet $\varphi_p(x)$.
- The support of $\phi_{j,k}$ is compact, *i.e.* $\text{supp}\{\phi_{j,k}\} \sim |O(2^{-j})|$.
- $\phi_{j,k}(x_{j,n} = n2^{-j}) = \delta_{k,n}$, *i.e.* satisfies the *interpolation property*.
- $\psi_{j,k} = \phi_{j+1,2k+1}$.
- $\text{span}\{\phi_{j,k}\} = \text{span}\{\{\phi_{j-1,k}\}, \{\psi_{j-1,k}\}\}$.
- $\{1, x, \cdots, x^{p-1}\}$, for $x \in [0,1]$, can be written as a linear combination of $\{\phi_{j,k},\ k = 0, \cdots, 2^j\}$.
- $\{\{\phi_{J_0,k}\}, \{\psi_{j,k}\}_{j=J_0}^{\infty}\}$ forms a basis of a continuous 1-D function on the unit interval $[0,1]$.

Sparse Wavelet Representation (SWR) and Irregular Sparse grid

- For a given threshold parameter ε, the multiscale approximation of a function $u(\mathbf{x})$ can be written as

$$
\begin{aligned}
u^J(\mathbf{x}) &= \sum_{\mathbf{k}} u_{J_0,\mathbf{k}} \Phi_{j_0,\mathbf{k}}(\mathbf{x}) + \sum_{j=j_0}^{J-1} \sum_{\{\boldsymbol{\lambda}\,:\,|d_{j,\boldsymbol{\lambda}}| \geq \varepsilon\}} d_{j,\boldsymbol{\lambda}} \Psi_{j,\boldsymbol{\lambda}}(\mathbf{x}) \\
&\quad + \underbrace{\sum_{j=j_0}^{J-1} \sum_{\{\boldsymbol{\lambda}\,:\,|d_{j,\boldsymbol{\lambda}}| < \varepsilon\}} d_{j,\boldsymbol{\lambda}} \Psi_{j,\boldsymbol{\lambda}}(\mathbf{x})}_{R_\varepsilon^J},
\end{aligned}
$$

  and the SWR is obtained by discarding the term R_ε^J.

- For interpolating wavelets, each basis function is associated with one dyadic grid point, *i.e.*

$$
\begin{aligned}
&\Phi_{j,\mathbf{k}}(\mathbf{x}) \quad \text{with} \quad \mathbf{x}_{j,\mathbf{k}} = (k_1 2^{-j}, \ldots, k_d 2^{-j}) \\
&\Psi_{j,\lambda}(\mathbf{x}) \quad \text{with} \quad \mathbf{x}_{j,\boldsymbol{\lambda}} = \mathbf{x}_{j+1,2\mathbf{k}+\mathbf{e}}
\end{aligned}
$$

SWR and Irregular Sparse Grid (continued)

- For a given SWR, one has an associated grid composed of *essential* points, whose wavelet amplitudes are greater than the threshold parameter ε

$$\boldsymbol{\mathcal{V}}_e = \{\mathbf{x}_{j_0,\mathbf{k}}, \bigcup_{j \ge j_0} \mathbf{x}_{j,\boldsymbol{\lambda}} \,:\, \lambda \in \boldsymbol{\Lambda}_j\}, \quad \boldsymbol{\Lambda}_j = \{\lambda \,:\, |d_{j,\lambda}| \ge \varepsilon\}.$$

- To accommodate the possible advection and sharpening of solution features, we determine the *neighboring* grid points:

$$\boldsymbol{\mathcal{V}}_b = \bigcup_{\{j,\boldsymbol{\lambda} \in \boldsymbol{\Lambda}\}} \mathcal{N}_{j,\boldsymbol{\Lambda}},$$

where $\mathcal{N}_{j,\boldsymbol{\lambda}}$ is the set of neighboring points to $x_{j,\boldsymbol{\lambda}}$.

- The new sparse grid, $\mathcal{V}$, is then given by

$$\boldsymbol{\mathcal{V}} = \mathbf{x}_{j_0,k} \cup \boldsymbol{\mathcal{V}}_e \cup \boldsymbol{\mathcal{V}}_b.$$

SWR and Irregular Sparse grid (continued)

- There exists an adaptive fast wavelet transform ($AFWT$), with $O(N)$, $N = \dim\{\boldsymbol{\mathcal{V}}\}$ operations, mapping the function values on the irregular grid $\boldsymbol{\mathcal{V}}$ to the associated wavelet coefficients and *vice-versa*:

$$AFWT(\{u(\mathbf{x}) \, : \, \mathbf{x} \in \boldsymbol{\mathcal{V}}\}) \to \mathcal{D} = \{\{u_{j_0,\mathbf{k}}\}, \{d_{j,\boldsymbol{\lambda}}, \; \boldsymbol{\lambda} \in \boldsymbol{\Lambda}_j\}_{j>j0}\}.$$

- Provided that the function $u(\mathbf{x})$ is continuous, the error in the SWR $u_\varepsilon^J(\mathbf{x})$ is bounded by

$$\|u - u_\varepsilon^J\|_\infty \leq C_1 \, \varepsilon.$$

- Furthermore, for the function that is smooth enough, the number of basis functions $N = \dim\{u_\varepsilon^J\}$ required for a given ε satisfies

$$N \leq C_2 \, \varepsilon^{-d/p}, \quad \text{and} \quad \|u - u_\varepsilon^J\|_\infty \leq C_2 \, N^{-p/d}.$$

Derivative Approximation of SWR

➢ Direct differentiation of wavelets is costly (with $O(p(J - j_0)N)$ operations) because of different support sizes of wavelet basis on different levels.

➢ Alternatively, we use finite differences to approximate the derivative on a grid of irregular points. The procedure can be summarized as follows:

1. For a given SWR of a function, perform the inverse interpolating wavelet transform to obtain the function values at the associated irregular points.
2. Apply locally a finite difference scheme of order n to approximate the derivative at each grid point.

➢ Estimate shows that the pointwise error of the derivative approximation has the following bound:

$$\|\partial^i u/\partial x^i - D_x^{(i)} u_\varepsilon^J\|_{\boldsymbol{\mathcal{V}},\infty} \leq C N^{-\min((p-i),n)/2}, \quad \|f\|_{\mathcal{G},\infty} = \max_{\mathbf{x}\in\boldsymbol{\mathcal{V}}} |f(x)|.$$

Dynamically Adaptive Algorithm for Solving Time-Dependent PDEs

Given the set of PDEs

$$\frac{\partial u}{\partial t} = F(t, u, u_x, u_{xx}, \ldots),$$

with initial conditions

$$u^0 = u(x, 0).$$

❶ Obtain sparse grid, $\boldsymbol{\mathcal{V}}^m$, based on thresholding of magnitudes of wavelet amplitudes of the approximate solution u^m.

❷ Integrate in time using an explicit time integrator with error control to obtain the new solution u^{m+1}.

❸ Assign $u^{m+1} \to u^m$ and return to step ❶.

Compressible Reactive Flow

Code solves the n-D compressible reactive Navier-Stokes equations:

$$
\begin{aligned}
\frac{\partial \rho}{\partial t} &= -\frac{\partial}{\partial x_i}(\rho u_i) \\
\frac{\partial \rho u_i}{\partial t} &= -\frac{\partial}{\partial x_j}(\rho u_j u_i) - \frac{\partial p}{\partial x_i} + \frac{\partial \tau_{ij}}{\partial x_j} \\
\frac{\partial \rho E}{\partial t} &= -\frac{\partial}{\partial x_j}(u_j(\rho E + p)) + \frac{\partial u_j \tau_{ji}}{\partial x_i} - \frac{\partial q_i}{\partial x_i} \\
\frac{\partial \rho Y_k}{\partial t} &= -\frac{\partial}{\partial x_i}(u_i \rho Y_k) + M_k \dot{\omega}_k - \frac{\partial j_{k,i}}{\partial x_i}, \qquad k = 1, \ldots, K
\end{aligned}
$$

Where ρ-density, u_i-velocity vector, E-specific total energy, Y_k-mass fraction of species k, τ_{ij}-viscous stress tensor, q_i-heat flux, $j_{k,i}$-species mass flux, M_k- molecular weight of species k, and $\dot{\omega}_k$-reaction rate of species k.

Compressible Reactive Flow (cont.)

Where,

$$
\begin{aligned}
E &= e + \frac{1}{2} u_i u_i \\
\tau_{ij} &= -\frac{2}{3}\mu \frac{\partial u_l}{\partial x_l}\delta_{ij} + \mu \left(\frac{\partial u_i}{\partial x_j} + \frac{\partial u_j}{\partial x_i} \right) \\
q_i &= -\mathsf{k}\frac{\partial T}{\partial x_i} + \sum_{k=1}^{K} \left(h_k j_{k,i} - \frac{RT}{m_k X_k} D_k^T d_{k,i} \right) \\
j_{k,i} &= \frac{\rho Y_k}{X_k \overline{M}} \sum_{j=1, j\neq k}^{K} M_j D_{kj} d_{j,i} - \frac{D_k^T}{T}\frac{\partial T}{\partial x_i} \\
d_{k,i} &= \frac{\partial X_k}{\partial x_i} + (X_k - Y_k)\frac{1}{p}\frac{\partial p}{\partial x_i}
\end{aligned}
$$

Project Challenges

- To maintain time accuracy, time step is restricted by finest spatial grid size.
- We need better time integration strategies, *i.e.* multiple time stepping or a time-adaptive method.
- Parallel domain decomposition and load balancing is challenging on an adaptive grid.
- Verified solutions with large geometries require large computational resources, even with an adaptive method.
  Powers and Paolucci *AIAA J* 2005; Powers *JPP* 2006

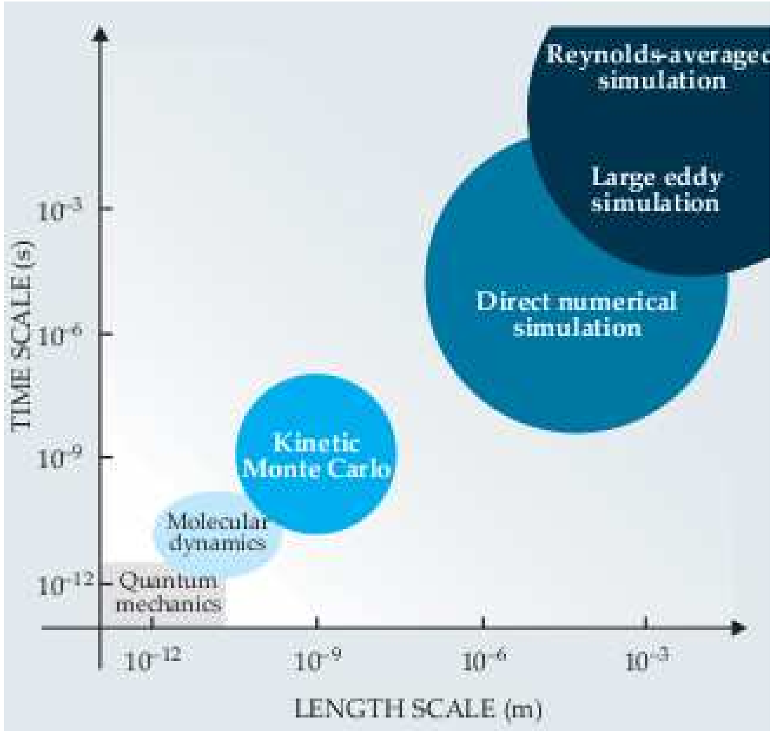

"Research needs for future internal combustion engines," *Physics Today*, Nov. 2008, pp 47-52.

Future Work

- ➢ Perform coarse-grained message passing-based parallelization.
- ➢ Improve data structure, maintaining constant-time data access.
- ➢ Implement non-reflecting boundary conditions for problems in open domains.
- ➢ Include generalized coordinates/domain transformation for non-Cartesian geometries.

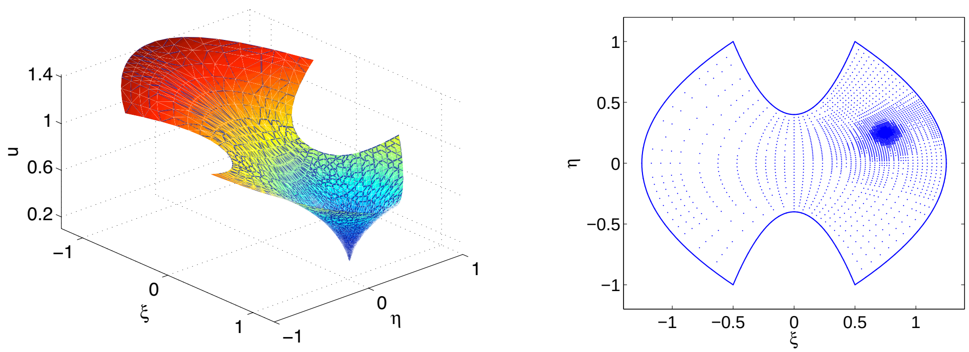

Figure: Solution and adaptive grid for a test problem in an irregular domain.

- ➢ Solve more complex problems with good experimental databases for validation.